ARTICLES

Exciton Mobility and Trapping in a MALDI Matrix

Patrick D. Setz[†] and Richard Knochenmuss*[,‡]

Laboratorium für Organische Chemie, Eidgenössische Technische Hochschule Zürich, 8093 Zurich, Switzerland, and Novartis Institutes for Biomedical Research, WSJ 503.1104, 4002 Basel, Switzerland

Received: February 4, 2005

Energy transfer (ET) from excited matrix to fluorescent traps is used to probe the mobility of excitations in the matrix-assisted laser desorption/ionization (MALDI) matrix material 2,5-dihydroxybenzoic acid. The dependence of host and guest fluorescence on excitation density (laser intensity) and trap concentration gives clear evidence for long-range energy transport in this matrix. This conclusion is further supported by time-resolved emission data showing a 2 ns delay between matrix and trap emission. Rate equation and random walker models give good agreement with the data, allowing determination of hopping, collision, and trapping parameters. Long-range energy transfer contributes to the pooling reactions which can lead to primary ions in MALDI. The results validate the pooling aspect of the prior quantitative MALDI ionization model (*J. Mass Spectrom.* **2002**, *37*, 867−877). It is shown that exciton trapping can decrease MALDI ion yield, even at low trap concentration.

Introduction

Matrix-assisted laser desorption/ionization (MALDI) has become a widely utilized analytical tool, yet was developed in a largely empirical fashion. Only recently has a fundamental understanding of MALDI with ultraviolet laser excitation begun to take form. Although some questions remain regarding the contribution of "preformed" ions[1,2] or pathways involving condensed ejecta,[3,4] only one model has proven capable of quantitatively accounting for a wide range of MALDI phenomena. In this model primary ionization processes are followed by secondary ion−molecule reactions in the plume.[5−8]

The primary ionization pathway was proposed to involve energy pooling by two excited matrix molecules.[7] This type of process has long been known in condensed systems[9−11] and is a result of the relatively strong interactions between aromatic π-electron systems when packed closely in a solid. The original model considered the probability that two laser-excited molecules would randomly be next to each other. By fitting experimental fluorescence quenching and MALDI time-delayed 2-pulse data,[12,13] empirical rate constants for static neighbor pooling processes were determined. These proved to be quite satisfactory and the model gives excellent results for many aspects of MALDI ion and electron generation.[5−8]

The possibility remained, however, that the dynamics of pooling were not fully described in this picture. Excitations can behave as mobile pseudoparticles (excitons) in solids, resulting in long range energy transport. The wave function of the excitation may be strongly localized on individual molecules or delocalized over several. The motion may be isotropic or highly directional, depending on the nature of the relevant intermolecular interactions in the crystal.[14,15] Demonstration of exciton motion in matrix materials would underscore the importance of pooling, since it is obviously more likely that excitations will interact if they can move about. It would also lead to a more accurate description of energy conversion and ionization during the first few nanoseconds of the MALDI process.

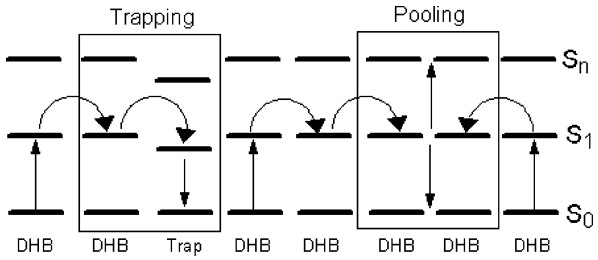

Figure 1. Schematic of the exciton hopping and pooling processes investigated here.

Fluorescence quenching experiments on pure matrix were fully consistent with a pooling process.[12] Quenching was roughly dependent on the second order of the laser fluence and hence the number of excitations in the solid.[6,12] This does not, however, differentiate between mobile excitons that "collide" or static excitations that are accidental neighbors.

Here we use fluorescent traps in the matrix crystal as a probe of excition motion. As illustrated in Figure 1, if the lowest excited state of an impurity molecule lies below that of the host molecules, a host exciton can be trapped by the impurity. After host-trap energy transfer has occurred, the trap may emit its own characteristic fluorescence. The intensity of this fluorsecence may be anomalously high if excitons are mobile and are frequently trapped before they emit or nonradiatively decay.

* To whom correspondence should be addressed. E-mail: richard.knochenmuss@novartis.com.
[†] Eidgenössische Technische Hochschule Zürich.
[‡] Novartis Institutes for Biomedical Research.

10.1021/jp050622c CCC: $30.25
Published on Web 04/15/2005

The density of excitons and traps are clearly important in determining the rate of trapping and hence the trap fluorescence. Laser fluence and trap concentration can therefore be varied to determine if excitons are mobile and how they move. In addition, mobile excitons may take significant time to move from the point of generation by the laser to the nearest trap. As a result, trap fluorescence may be delayed compared to that of the matrix. All of these diagnostics for exciton mobility are applied here, and are found to indicate mobile excitons in the matrix 2,5-dihydroxybenzoic acid.

In addition, we present results of numerical models for exciton motion and trapping under MALDI-relevant conditions. These simulations not only allow interpretation of the data, but provide dynamical information of fundamental interest for the MALDI ionization model.

Experimental Section

The MALDI matrix 2,5-dihydroxybenzoic acid (DHB) was obtained from Fluka, Buchs, Switzerland. It was purified by repeated recrystallization from water and methanol. The laser-grade dye DCM was obtained from Radiant Dyes GmBH, Friedrichstrasse 58, Wermelskirchen, Germany, and was used as received. Single crystals of DHB and DHB doped with DCM were grown by slow evaporation of ethanol−water (v/v 1:5) solutions. They were as large as $2 \times 2 \times 1$ mm. The doped crystals were thoroughly washed with cold chloroform to remove any residual dye adsorbed on the crystal surface. DHB was found to be insoluble in this solvent, whereas DCM remained soluble. This ensured that the fluorescence experiments measured only DCM incorporated in DHB. The crystals were then dried and stored under vacuum.

The DCM concentrations in the mother liquor ranged from 10^{-5} to 10^{-10} M. At DCM concentrations higher than 10^{-5} M, the crystals were inhomogeneously colored. This upper limit for uniform dopant incorporation is in good agreement with studies of protein incorporation in MALDI matrixes.[16]

The true DCM concentrations in the crystals was determined colorimetrically after the fluorescence experiments were completed, by dissolving the crystals in ethanol.

Solution phase absorption spectra were acquired using an Ocean Optics PC2000 diode array spectrophotometer, and emission spectra were measured on a Perkin-Elmer LS-50 fluorimeter.

Solid-state absorption spectra were measured with the Ocean Optics spectrometer and a fiber backscattering probe (R400-7). The probe consisted of 6 illumination fibers surrounding one detection fiber. Thin samples were prepared by the dried droplet method on aluminum foil. This sample was placed under a aluminum sampling cone, on top of which the fiber probe could be inserted. This cone completely isolated the sample from ambient light. The end of the fiber was 5 mm from the sample. Spectra were referenced to uncoated aluminum foil.

The solid state emission spectra were obtained in a specially constructed apparatus. The crystal under study was mounted on a support rod which was inserted into a vacuum chamber. The rod could be rotated and axially translated to obtain the best signal. The vacuum was typically 10^{-5} mbar, to simulate MALDI conditions.

Near-UV light at 355 nm was generated by frequency tripling of the fundamental of a Continuum PL7020 Nd:YAG laser. The laser was injection seeded to obtain a smooth temporal pulse of 5−7 ns duration. The laser was coupled into a 8 m, 0.55 mm dia. fused silica fiber (Type FG550 UER, Thorlabs) which transported the beam to the fluorescence setup. It also served to spatially homogenize the beam, providing a "flat-top" profile on the sample.[17]

After leaving the fiber, the beam was collimated, and the pulse energy was measured either directly by a pyroelectric element (ED-100A, Gentec) or indirectly using a window reflection and a photodiode which was calibrated against the pyroelectric detector. The beam then passed through a $f = 15$ cm focusing lens outside the vacuum system. The converging beam entered the experimental chamber through a silica window and was then redirected by a prism system so as to impinge on the sample at a shallow angle to the observation axis. This provided a nearly circular laser spot. The laser spot size was measured using ablation of ink films, thermal paper, or desorption craters on DHB crystals.

The emitted light was collected by a f/4 system comprising 2 lenses and dispersed by a 0.5 m grating monochromator (SPEX 500M). For spectroscopic measurements, the spectrum was imaged onto a Princeton LN/CCD-2500-PB/VISAR detector array. The response of the CCD/spectrometer system was characterized using a calibrated lamp.

The time-resolved measurements were obtained with a Hamamatsu R3896 photomultiplier tube (rise time at 1000 V: 2.2 ns, spectral response 185−900 nm, max at 450 nm) on the second output port of the monochromator. This output was equipped with a slit for wavelength selection. A LeCroy LC 584 A digital oscilloscope was used to collect the data, operating at 8×10^9 samples per second. The oscilloscope was triggered using a fast photodiode at the laser, which sampled a small amount of the 355 nm beam. Laser light scatterd from a metal plate was used to obtain an instrument response function, which was used to deconvolute the fluorescence signals. Repeated measurements of the laser pulse were made, to verify the stability of laser and trigger.

MALDI mass spectra were recorded on an Applied Biosystems Voyager DE STR (Applied Biosystems Framingham, MA), in reflectron mode with delayed extraction. Each spectrum is the sum of 200 laser shots (355 nm). Each crystal was sampled at several spots, the results shown are from the spot yielding the highest signal.

Results and Discussion

Absorption spectra of DHB and DCM in solution and in the solid state are shown in Figure 2. The spectra broaden somewhat in the solid phase vs solution,[18] but the basic features remain the same, and the two absorptions are well separated. Laser irradiation of a mixed crystal of DCM in DHB at 355 nm results predominantly in excitation of the DHB host. Comparing Figure 2 with the emission spectra of Figure 3, it is apparent that the DHB fluorescence has considerable overlap with the DCM absorption band. Resonant energy transfer from DHB to DCM is therefore possible. As a consequence of these characteristics, this host/trap pair was considered a good system for study of exciton mobility and trapping.

As shown in Figure 3, DCM trap fluorescence is strong even at low concentrations in DHB. The radiative yields of host and guest are equal at 10^{-6} to 10^{-7} M. Since DCM was selected for low absorption at the excitation wavelength, this is a strong indicator of exciton transport in DHB host crystals. Even if DCM had a 10 times greater quantum efficiency than DHB, and it absorbed 10% of the incident light (i.e., had an absorption cross section 10^5 greater than that of DHB), the relative DCM emission should still be only 10^{-4} to 10^{-5} at these concentrations. The observed ratio of about 1 is then still 100−1000 times

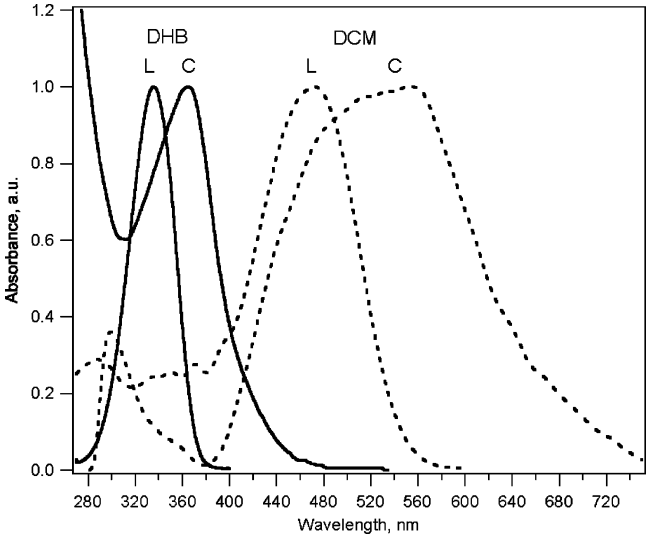

Figure 2. Absorption spectra of DHB (solid lines) and DCM (dashed lines), the host and trap substances used in this study. L, in ethanol liquid solution; C, in crystalline form.

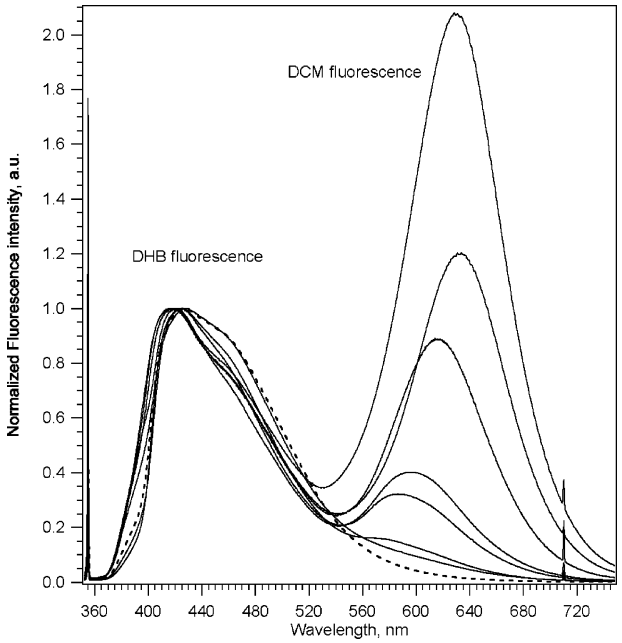

Figure 3. Fluorescence spectra of DHB crystals doped with DCM. The spectra have been normalized to the DHB fluorescence maximum. The dashed line corresponds to an undoped DHB crystal. The laser generates the sharp line on the left edge of the figure (355 nm), and the second-order diffraction of this appears as a peak near the right edge. The DCM concentration in the crystals was (from bottom to top): 2×10^{-9}, 5×10^{-9}, 3×10^{-8}, 4×10^{-8}, 2×10^{-7}, 3×10^{-6}, and 4×10^{-6} M.

too strong to be explained by direct absorption of the laser. The bulk of the emission must be a result of excitation energy transfer from excited matrix.

This can be constrasted with the control experiment in which DHB and DCM were ground together at similar mole ratios, and the emission from the fine powder was recorded. As seen in Figure 4, the relative DCM fluorescence is considerably weaker than that observed from the grown crystals. This shows dramatically that DCM is incorporated in the DHB crystals, leading to energy transfer and trapping.

At 10^{-6} trap:host mole ratio, uniformly distributed traps are separated by 100 host diameters. At the moderate laser intensities used for this measurement, and for an absorption cross

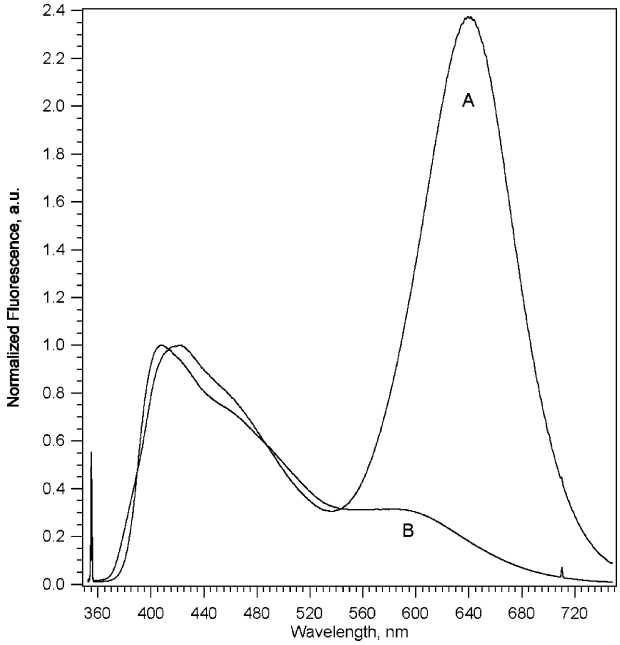

Figure 4. Fluorescence spectra of a crystal of DHB doped with DCM (A) and DHB ground with DCM (B). The former exhibits much stronger DCM fluorescence. The molar ratio of DHB to DCM was 10^3 in both cases, although the mixed crystal very probably did not incorporate this much DCM.

section of 10^{-17} cm^2,[19] the number of matrix excitations reaches a maximum on the order of 1000 per trap. The matrix quantum efficiency in the solid is about 1/30 (from the measured solid vs gas-phase fluorescence lifetimes, assuming the 30 ns molecular beam result to be the intrinsic lifetime),[12] so 33 matrix fluorescence photons would be expected from the volume around one trap.

Trap fluorescence depends on the range of energy transfer from the host. The shortest range is the distance to the nearest neighbors. If located at a cubic site, a trap has 6 nearest neighbors, so its probability of trapping a static matrix excitation is 6 neighbors $\times$ (1000 excitations per 10^6 sites), or 6×10^{-3}. The expected trap:matrix fluorescence ratio at this trap concentration is then $6 \times 10^{-3}/33$ or about 1:5000. Since the observed ratio is about 1:1, this means that the traps are able to "collect" excitons from a larger volume than just their nearest neighbors. Energy transfer is efficient over about 17 ($=5000^{(1/3)}$) molecular diameters. Hopping distances of this order are known from other systems.[11,20] This is too far to be due to fluoresecence resonance energy transfer (FRET) from the laser excited matrix directly to DCM, as will be discussed below.

Another strong indicator of transport and trapping is shown in Figure 5. The time and wavelength resolved trap emission is shifted to later times than that of the host matrix. The delay in the peak of the emission is 2−3 ns. Not only is the peak delayed but also the rising edge of the DCM emission. This is very strong evidence that the traps are not being significantly directly excited. They emit only after the excitation energy has had time to migrate in the DHB crystal. As also shown in the figure, the trap emission is slower than from pure DCM. This is another indication that the traps are incorporated into the DHB crystal and not present as aggregates on the surface or as inclusions.

The time-resolved data were analyzed with a fitting procedure that convoluted the measured response to the laser pulse with a single exponential. As expected, a single exponential is often inadequate to simultaneously fit all parts of either the host or guest emissions. Exciton diffusion and trapping lead to devia-

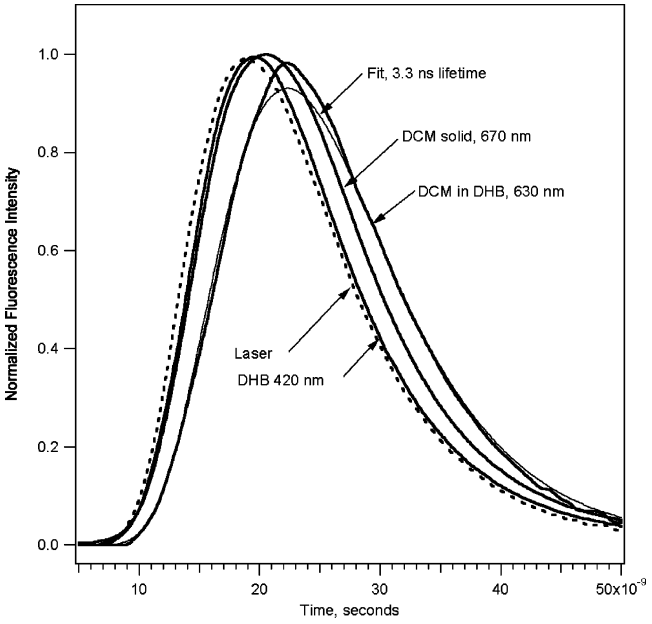

Figure 5. Time-resolved emission of solid DHB and both DHB and DCM (4×10^{-8} M) in a mixed crystal at the indicated wavelengths. The laser fluence was 0.1 J/m^2. The instrument response to a 355 nm laser pulse scattered from a metal surface is also shown (dashed line). The fit curve results from the trapping differential equations described in the text.

tions from such simple behavior as energy is transferred from one to the other. However, the falling flank of the trap signal should approach exponentiality, after the bulk of the trapping has occurred. This was observed. Good exponential fits were obtained for the DCM emission at longer times, with a time constant of 3−4 ns. This did not change with fluence over the range 0.1−200 J/m^2. Fits for the DHB emission were more difficult since the differences with the laser pulse response were smaller. However, results in the range of ≤1 ns were obtained, below those of Lüdemann et al.[12] Other authors have also found short DHB lifetimes in the solid state.[21] The rising edge was slower than the falling flank, as expected for delayed trapping. Typical values were as follows: leading flank, 0.64 ns; trailing flank, 0.25 ns.

The mean time to trapping is approximately the 2 ns delay between host and trap emission. If isotropic, the mean diffusion distance as a function of time after creation of an exciton is[22]

$$D(t) = d_h\sqrt{t/\Delta t_h}$$

where d_h is the distance moved in one hop, Δt_h is the time for one hop, and t is the total diffusion time. The trapping distance, D(2 ns), was estimated above at about 17 molecular diameters, leading to a hop time of 7×10^{-12} s. This should be considered a lower bound, since it is not rigorous in a case like this where pooling also plays a role and does not take into account other processes such as quenching at nonfluorescent sites such as crystal defects.

More detailed analysis involves numerical models. The first uses differential rate equations for the ground (M_0, T_0) and first excited (M_1, T_1) singlet states of both matrix (M) and trap (T). The laser excites only the matrix, and the excited matrix can transfer energy to traps. Detrapping of an excited trap to reform a matrix exciton is not included. Pooling is accounted for by quadratic terms in the matrix excitons. Consistent with the full MALDI model, pooling leaves one matrix molecule in a higher excited state, whereas the second is deactivated to the ground state. Since nonradiative decay of the higher excited state is rapid compared to that of the M_1, this step can be neglected here, and one of the pooling partners simply remains in the original M_1 state. The relative fluorescence intensities of matrix and trap depend on the time-integrated M_1 populations and the respective quantum efficiencies.

$$\frac{dM_0}{dt} = \frac{M_1}{\tau_M} + k_{trap}M_1T_0 - \sigma IM_0 + k_{pool2}M_1M_1 + 3k_{pool3}M_1M_1M_1$$

$$\frac{dM_1}{dt} = \frac{-dM_0}{dt}$$

$$\frac{dT_0}{dt} = \frac{T_1}{\tau_T} - k_{trap}M_1T_0 - \left(\frac{\sigma}{10}IM_0\right)$$

$$\frac{dT_1}{dt} = \frac{-dT_0}{dt}$$

where σ is the matrix absorption cross section and I is the laser intensity, taken to have a 5 ns Gaussian temporal profile. The excited-state lifetimes are τ_M and τ_T. The last trap term of the third equation is in parentheses to indicate that weak direct trap absorption was also considered but found unnecessary for a good fit.

For low excitation densities the trapping rate was given by

$$k_{trap} = \text{capture factor} \times [T_0]/[T_0 + T_1]/\text{hoptime}$$

where the capture factor represent the trapping volume of a single trap. For a trapping radius of 10 as determined above, this is 10^3. The time-dependent factor $[T_0]/[T_0 + T_1]$ accounts for depletion of the trap ground state.

At higher excitation densities, it is likely that more than one matrix excitation is near each trap. This is approximately accounted for by an extra factor of

$$[M_1]/[T_0 + T_1]$$

when ever this factor was greater than unity.

The first test for this model is to reproduce the fluence-dependent fluorescence quenching of pure matrix. The full UV-MALDI model was partially calibrated using this observable, and with the data from ref 12 Including only the binary pooling term ($k_{pool3} = 0$), the above equations reproduce these data well, as expected, and shown in Figure 6. The bimolecular rate constant from this fit was 7×10^9 s^{-1}, multiplied by 27 neighbors (nearest and next-nearest). The value used in ref 6 was also 7×10^9 s^{-1}, but only the 6 nearest neighbors were considered. This may be compared to better known systems such as anthracene, where the rate is much higher, above 10^{13} s^{-1}.[11]

The data of ref 12 suffered from truncation at lower fluence. Without a clear region of zero slope at low fluence, it was not certain if the data could be legitimately scaled to unity at the low end. Because of this, we made similar measurements over a wider fluence range. The region where no nonlinear effects occur is now clearly defined, as seen in Figure 6. (The earlier data have been scaled for best agreement with the new measurements.) Surprisingly, however, in the high fluence region, the two data sets do not coincide.

Repeated attempts to identify an experimental reason for this difference were unsuccessful. In particular, the possibility of nonfluorescent quenching impurities was considered, and the DHB was repeatedly purified. The form of the curve remained as in Figure 6. Finally, it was concluded that the steeper drop

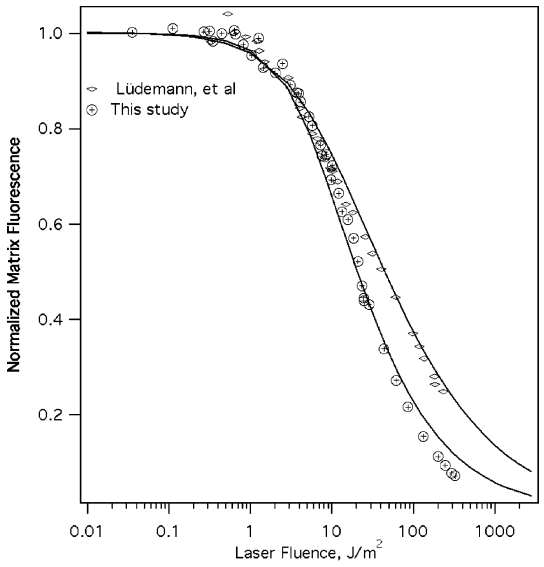

Figure 6. Normalized DHB fluorescence vs laser fluence. Both the data of this study (round symbols) and that of ref 12 (diamonds) are shown. The fit curves result from the differential equations described in the text.

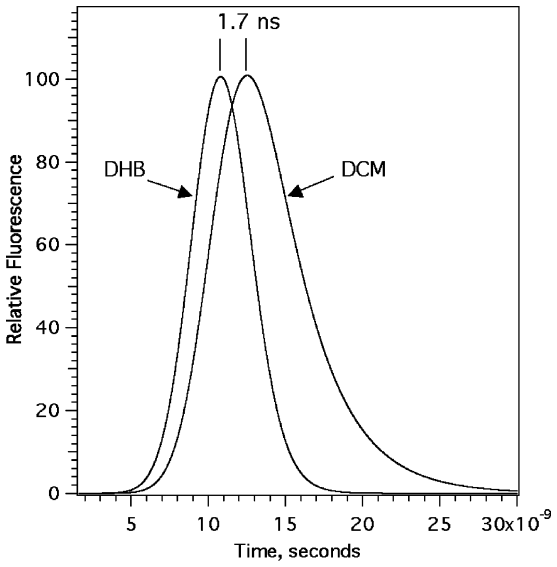

Figure 7. Time-resolved emission from DHB crystals doped with DCM, as predicted by the differential equations described in the text.

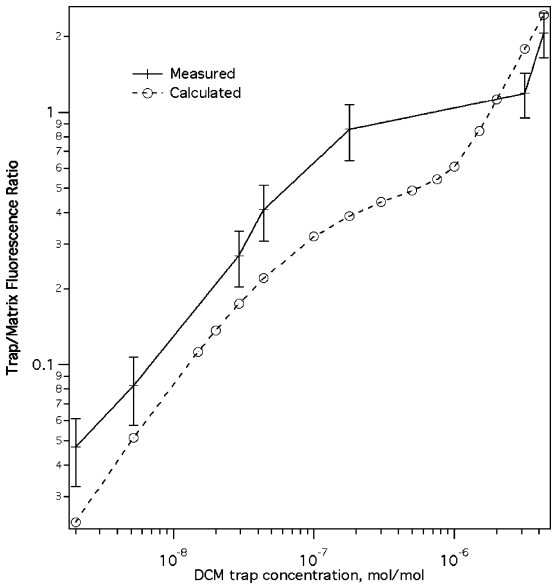

Figure 8. Ratio of DCM to DHB fluorescence vs DCM concentration in doped crystals. The dashed line is predicted by the differential equations described in the text.

at high fluence may well be a reflection of exciton mobility and pooling, which can be more efficient in crystals of higher purity. A term of higher than second order is necessary to explain the steeper drop, the curve through the newer data in Figure 6 includes a term for triple pooling, $k_{pool3} = 5 \times 10^{13}$ s^{-1}.

The need for triple pooling supports the hypothesis of exciton mobility since the fluences here were insufficient for large amounts of triply excited clusters to exist by random laser excitation (probability $\approx 10^{-4}$ at 100 J/m^2). Also, if this were not the case, this term would be necessary to fit the Lüdemann data as well. The newer data appear to need it because the DHB was highly purified. Nonfluorescent scattering impurities limit the range of matrix excitons by blocking transfer, leading to isolated regions which have little or no contact with each other. The local excitation density in these regions then determines the pooling behavior. If scattering sites are sufficiently numerous, then regions with more than 2 excitons become rare. With unhindered motion or larger regions, it becomes possible for ternary pooling processes to take place at their natural rate, as excitons move on the extended lattice.

In this model, the trapping range is implicit in the rate constants rather than explicit in the form of the equations. If trapping takes place over the same range as pooling, the trapping rate constant can be no larger than the pooling constant, because both trapping and pooling are measures of how often a given exciton encounters other species. For pooling these are other excitons, for trapping it is a ground-state trap (which is then raised to the first excited state by the trapping event). To reflect a larger trapping rate due to longer range energy transfer, the rate constant is multiplied by a factor representing the volume of matrix which is "emptied" by each trap. For a trapping range of 10, this would be 10^3. This parameter affects not only the relative efficiency of trap emission but also the time dependence of exciton-trap energy transfer. Larger trap regions obviously imply faster and more efficient trapping.

Retaining the triple pooling term, and adding traps, the time dependence of DHB and DCM emission are directly obtained from integration of the rate equations. The DCM apparent (not intrinsic) radiative lifetime in DHB host was taken to be 3 ns, as estimated from the fits to the data described above. As seen in Figure 7, the delay of the DCM fluorescence vs that of DHB is well reproduced by the model. It should be recalled that if the DCM emission were the result of direct laser excitation, the 640 nm signal would rise concurrently with that of DHB at 420 nm. These results were obtained with a trapping range of 10 sites, not far from the 17 estimated above from the fluorescence intensity ratios.

With the trapping and decay parameters determined up to this point, it is possible to calculate the trap:host fluorescence ratio over a range of trap concentrations. Experimentally, a nonlinear dependence is found, as shown in Figure 8. The shape predicted by the model depends on the laser fluence, since this affects the typical distance to the nearest trap. At a fluence of 3.5×10^{-4} mJ/cm^2, the calcuation gives a similarly shaped curve, although agreement is not quantitative. That this nonlinearity can be qualitatively reproduced is considered another significant indication that hopping is the mechanism of energy transport, since other mechanisms such as FRET do not yield such a shape.

The rate equation model has proved to be remarkably successful in treating the data presented here. In a certain sense, this is surprising since exciton trapping is not always amenable to such a treatment. Somewhat similar to time-dependent collision rates in diffusion (Smoluchowski equation),[23] the trapping rate for a given individual exciton is not constant. After creation by the laser, the volume sampled, and hence the probability of trapping, increases with time. In the limit of low exciton density, i.e., no exciton−exciton interaction and many more traps than excitons, this leads to nonexponential behavior that is not predicted by the rate equations above.[24−26] However, exciton densities in MALDI matrixes at MALDI-relevant laser fluences are far from low, as is evident from the pronounced fluorescence quenching. To our knowlege, there appears to be no trapping theory currently available which is valid for such conditions. To evaluate the possible role of time-dependent rates in MALDI matrixes, the motion and trapping of excitons was therefore numerically simulated.

A cubic volume of matrix molecules was considered, containing a few 10^6 to $>10^{10}$ molecules. These sizes were necessary for inclusion of significant numbers of traps at the low concentrations used in the experiments. At each time step, random sites were laser excited, at a rate determined by the shape and intensity of the laser pulse. These were allowed to move up to one lattice spacing in any direction at each step, in a random direction. At each step, the proximity of each exciton to others and to traps was checked. One simulation step was therefore equivalent to the exciton hop time. Periodic boundary conditions in all three dimensions were applied to the motion and to pooling or trapping. Those excitons within the specified range were pooled or energy was transferred to the traps, respectively. Both matrix and trap were allowed to fluoresce with lifetimes as determined above. With well adapted proximity algorithms, it was possible to simulate intense laser pulses generating millions of excitons for time periods of tens of nanoseconds.

Key parameters in this model are the exciton hop rate, the pooling and trapping radii, the excited state lifetimes, and the probability that two excitons that meet will pool. The lifetimes and trapping radius were all previously estimated. The hopping rate, pooling probability, and pooling radius were adjusted for best agreement with the data. Triple pooling was considered too computationally intensive for the large volumes considered, so the matrix quenching data of Lüdemann was fit, rather than the newer data.

As seen in Figure 9, agreement with the quenching data was good, using a hopping time of 5×10^{-11} s, a pooling radius of 2 molecules, and a pooling probability of 0.5. With these matrix parameters, and a trapping radius of 10, the time dependence of trap vs matrix fluorescence is also well predicted, as is the trap/matrix fluorescence ratio at high trap concentration.

Regarding deviations from the rate equation approach, Figure 10 shows the pooling rate vs excitation density. It has a quadratic dependence, and there are no indications of problematic behavior due to exciton motion at any exciton density. The pooling rate constant which corresponds to this curvature is 1×10^{12} s^{-1}. Normalized to the pooling volume, this becomes 1.5×10^{10} s^{-1}, which corresponds reasonably well with the value used in the full MALDI model of 7×10^9 s^{-1}.[5,6] The 5×10^{-11} s hopping time is rather slow compared to other, well studied systems. For example, the hopping rate in naphthalene crystals is on the order of 10^{-12}−10^{-13} s.[20]

An implication of the results presented here pertains to analyte fragmentation in MALDI. For those analytes which have excited states below the S_1 of the matrix, energy transfer from the matrix may be efficient. Labile molecules may directly dissociate as a result. Others may undergo efficient nonradiative decay, with consequent increased local heating. Increased fragmentation rates could again be the result.

Energy transfer to analytes can also reduce MALDI ion yields by reducing exciton populations and hence the rate of pooling reactions. This is demonstrated in Figure 11 for DCM in single crystals of DHB. At constant laser power, ion signals decrease significantly as DCM concentration is increased, although DCM concentrations are, by usual MALDI standards, quite low and

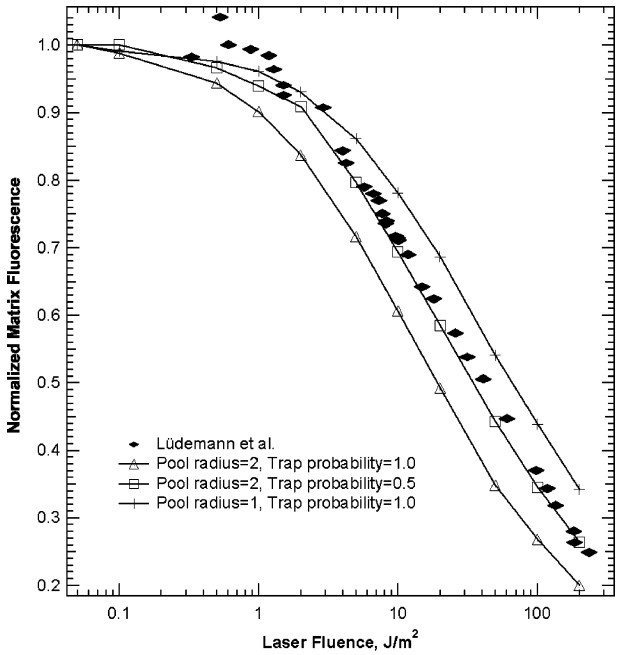

Figure 9. Normalized DHB fluorescence vs laser fluence. Only the data of ref 12 (diamonds) are shown. The fit curves result from the random walker model described in the text. In each case the exciton hop time was 5×10^{-11} s. From bottom to top, the other parameters are as follows: pool radius 2 diameters, pool probability 1.0; pool radius 2 diameters, pool probability 0.5; pool radius 1 diameter, pool probability 1.0.

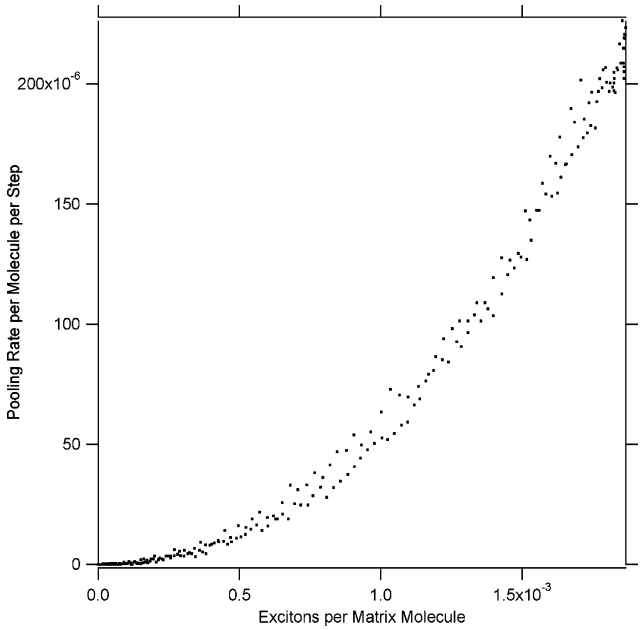

Figure 10. Pooling rate vs exciton density, as calculated using the random walker model described in the text.

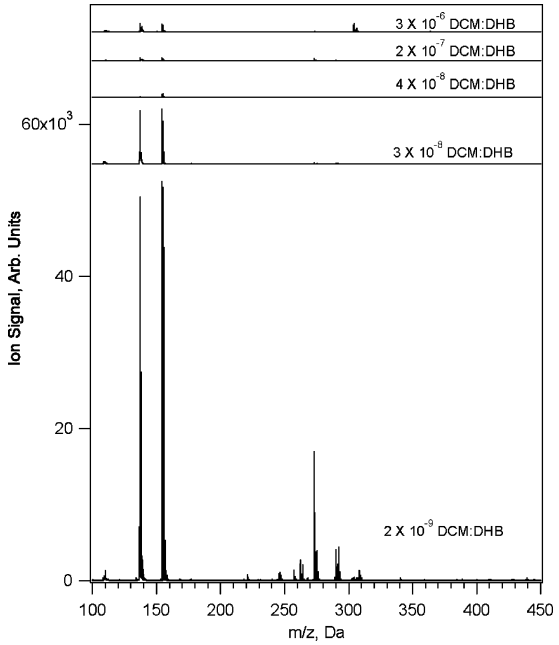

Figure 11. MALDI-TOF mass spectra of DHB single crystals doped with DCM laser dye. The laser intensity was identical for all spectra, and the spectra are plotted on the same vertical scale for comparison. Even at low concentrations, DCM quenches ion formation.

much too low for the matrix suppression effect.[5] Increased laser power, and consequently higher exciton density, can restore the signal, but only to a limited degree. Different crystals of the same nominal trap concentration also give varying signals, but higher concentrations gave consistently weaker spectra. Fortunately, exciton quenching is not a common phenomena in most MALDI applications since such strong chromophores with low-lying excited states are not often encountered in biomolecular systems such as proteins and peptides, or synthetic polymers.

FRET vs Hopping as an Energy Transfer Mechanism. For the sake of clarity, the above discussion focused on hopping as the energy transport mechanism to traps. Although exciton motion is common in condensed aromatics, it is less familiar than fluorescence resonance energy transfer (FRET), which is widely used as a local distance measure in molecules or molecular complexes, particularly in biological systems. We here discuss reasons why FRET is considered much less likely than exciton motion in the system DHB/DCM.

FRET is a long range transport mechanism, which is usually assumed to rely on dipole−dipole interactions. In the classical Förster treatment,[27] the rate has a $1/R^6$ dependence on distance from donor to acceptor. As a result, the distance for 50% transfer efficiency (R_0) is typically 3−6 nm, for optimized donor−acceptor pairs.[28] Using our measured absorption and fluorescence data for DHB crystal and DCM in solution, a R_0 distance of 2.9 nm is calculated. This assumes random orientation of the DCM vs DHB transition dipoles. Should the dipoles be optimally oriented in every case, R_0 rises to 3.9 nm.

These values are comparable to many other Förster pairs but are short compared to the range of energy transport demonstrated above. The DHB unit cell[29] is such that the estimated 17 molecule mean transport range corresponds to 8.4 nm, along the axis with the best π-electron overlap ($b = 0.491$ nm). This is 2−3 times the Förster R_0 distance. Along the *a* and *c* axes, the unit cell is larger, 2.395 and 0.562 nm, respectively. The 17 molecule range would be correspondingly larger if transport is also efficient in these directions.

The concentration dependence of the trap:host fluorescence is also an indication that hopping, and not FRET, is active. As noted in the discussion of Figure 8, the humped shape of the data could be qualitatively reproduced with a hopping model. Using the $R_0^6/(R_0^6 + R^6)$ Förster FRET rate dependence, no such concentration dependence could be generated. Either the trend was very close to linear or had a slight upward curvature, depending on the laser fluence.

FRET becomes more efficient as donor-trap spectral overlap increases. DHB crystals were also grown with a second laser dye, coumarin 153 (C153), as dopant. C153 has excellent overlap with the DHB emission, better than DCM. However, the trap fluorescence was much weaker at equal dopant concentrations than with DCM. Up to 1000 times higher nominal C153 concentration was necessary for the same trap:donor fluorescence ratio. This is not consistent with FRET, but is possible for hopping. When the trap excited state lies only slightly below that of the donor, detrapping via thermal energy competes with trap luminescence.[20] The trap depth for DCM is 40 kJ/mol deeper than that of coumarin 153 (from the fluorescence maxima), readily expaining the observed difference in trapping efficiency.

Finally, it should be noted that fluorescence quenching in trap-free (or at least not intentionally doped) DHB was found to be consistent with hopping. It would be surprising if hopping contributed to fluence-dependent quenching but not to trapping.

Conclusions

Fluence-dependent fluorescence quenching in pure DHB and energy transfer from the excited DHB matrix to fluorescent DCM traps were used to demonstrate that matrix excitations are mobile in DHB. DHB vs DCM fluorescence intensity ratios and time-resolved DHB vs DCM fluorescence are all consistent with this conclusion.

Two theoretical approaches were used to model the data. Both a rate equation method and direct simulation of exciton motion successfully reproduced the data. The exciton hopping time was estimated to be 5×10^{-11} s. The trapping radius for DCM in DHB is estimated to be 10−20 molecular diameters.

The results are particularly important for a full desciption of the pooling processes which are a key part of the quantitative MALDI model. The 2-exciton rate determined here, including exciton motion, is completely consistent with the earlier estimate used in that model A new discovery is the contribution of 3-exciton processes at high laser fluences. This process is dependent on unhindered exciton motion and is therefore only significant in unusually pure DHB.

Finally, exciton trapping was shown to affect ion yields in MALDI. DCM in DHB significantly reduced ion yields even at very low concentrations.

Acknowledgment. This work was partially supported by the Schweizerische Nationalfonds, grant nr. 21-63558-00.

Appendix

The hopping and trapping simulation is summarized here.

Key parameters are the hopping time, the laser pulse intensity and width, the absorption coefficient, the radiative lifetimes of matrix and trap, the quantum efficiencies of matrix and trap, the trap concentration, and the trapping radius.

Initialization: the traps are randomly distributed, according to the desired concentration. The total system size must be large enough that a statistically significant number of traps are present. Simulations of lower concentrations must therefore be larger.

The simulation step size is one hopping time. At each step, the following takes place:

(1) Laser photons impinge on the material, according to the selected pulse width and energy. The number absorbed depends on the absorption coefficient and the selected depth of the sample. If a randomly selected site already is excited, the photon is not absorbed.

(2) The proximity of excitons to traps is tested. Those within the capture radius give their energy to the trap (unless the trap is already excited).

(3) The excitons and traps are allowed to probabilistically decay, according to their lifetimes and quantum yields.

(4) Excitons are tested for proximity. Those within the specified radius undergo pooling. One is deactivated to the ground state. The other is, in reality, promoted to a higher state. This state is short-lived, so here the molecule is assumed to relax within 1 step back to the first excited state. Pooling therefore is a net reduction of the exciton population by one.

(5) The excitons move in a random direction, x, y, or z (or any combination), by −1, 0, or +1 step (randomly selected).

To facilitate the proximity testing in large simulation spaces, a linked list technique was used. Each excitation and trap was assigned to a spatial sub-cell. The cells were sufficiently large that only neighboring cells needed to be searched, not the entire space.

Periodic boundary conditions were used in all 3 dimensions.

References and Notes

(1) Kruger, R.; Pfenninger, A.; Fournier, I.; Glückmann, M.; Karas, M. *Anal. Chem.* **2001**, *73*.

(2) Karas, M.; Glückmann, M.; Schäfer, J. *J. Mass Spectrom.* **2000**, *35*, 1−12.

(3) Livadaris, V.; Blais, J.-C.; Tabet, J.-C. *Eur. J. Mass Spectrom.* **2000**, *6*, 409−413.

(4) Fournier, I.; Brunot, A.; Tabet, J.-C.; Bolbach, G. *Int. J. Mass Spectrom.* **2002**, *213*, 203−215.

(5) Knochenmuss, R. *Anal. Chem.* **2003**, *75*, 2199.

(6) Knochenmuss, R. *J. Mass Spectrom.* **2002**, *37*, 867−877.

(7) Knochenmuss, R.; Stortelder, A.; Breuker, K.; Zenobi, R. *J. Mass Spectrom.* **2000**, *35*, 1237−1245.

(8) Knochenmuss, R.; Zenobi, R. *Chem. Rev.* **2002**, *103*, 441−452.

(9) Northrop, N. C.; Simpson, O. *Proc. R. Soc. London* **1958**, *A244*, 377.

(10) Birks, J. B. *Photophysics of Aromatic Compounds*; Wiley-Interscience: London, 1970.

(11) Pope, M.; Swenberg, C. E. *Electronic Processes in Organic Crystals and Polymers*; Oxford University Press: Oxford, U.K., 1999.

(12) Lüdemann, H.-C.; Redmond, R. W.; Hillenkamp, F. *Rapid Comm. Mass Spectrom.* **2002**, *16*, 1287−1294.

(13) Knochenmuss, R.; Vertes, A. *J. Phys. Chem. B* **2000**, *104*, 5406−5410.

(14) Dexter, D. L.; Knox, R. S. *Excitons*; John Wiley & Sons: New York, 1965.

(15) Davydov, A. S. *Theory of Molecular Excitons*; McGraw-Hill: New York, 1962.

(16) Strupat, K.; Kampmeier, J.; Horneffer, V. *Int. J. Mass Spectrom. Ion Proc.* **1997**, *169/170*, 43−50.

(17) Schürenberg, M. Matrix-unterstützte Laserdesorptions/Ionisations-Massenspektrometrie (MALDI-MS) in optischer Invertgeometrie und mit Wellenlängen im sichtbaren Spektralbereich, Westfälische Wilhelms-Universität Münster, 1996.

(18) Dreiseverd, K. *Chem. Rev.* **2003**, *103*, 395−426.

(19) Allwood, D. A.; Dyer, P. E.; Dreyfus, R. W. *Rapid Commun. Mass Spectrom.* **1997**, *11*, 499−503.

(20) Braun, A.; Pfisterer, H.; Schmid, D. *J. Luminesc.* **1978**, *17*, 15−28.

(21) Zechmann, C.; Muskat, T.; Grotemeyer, J. **2002**, *8*, 287−293.

(22) Atkins, P.; de Paula, J. *Physical Chemistry*, 7 ed.; Oxford University Press: Oxford, U.K., 2002.

(23) Birks, J. B. *Organic Molecular Photophysics*; Wiley: New York, 1973; Vol. 1.

(24) Wong, Y. M.; Kenkre, V. M. *Phys. Rev. B* **1979**, *20*, 2438−2450.

(25) Rudemo, M. *J. Appl. Math.* **1966**, *14*, 1293−1297.

(26) Soos, Z. G.; Powell, R. C. *Phys. Rev. B* **1972**, *6*, 4035−4046.

(27) Förster, T. *Ann. Phys. Leipzig* **1948**, *2*, 55−75.

(28) Wu, P.; Brand, L. *Anal. Biochem.* **1994**, *218*, 1−13.

(29) Haisa, M.; Kashino, S.; Hanada, S.-I.; Tanaka, K.; Okazaki, S.; Shibagaki, M. *Acta Crystallogr.* **1982**, *B38*, 1480−1485.